Chapter 4: A Generalized Nusselt Number Correlation for Binary Hybrid Nano-oils as Heat Transfer Fluid

The literature review (see Table 2.2) reveals the unavailability of Nusselt number correlation for the turbulent flow of hybrid nano-oils. Also, the range of Prandtl numbers for water and oils is substantially different. Therefore, the exponents and coefficients appearing in Nu_{hnf} are expected to be different for oil and water as the base fluids, and the same is discussed in sub-section 4.1. Consequently, the water-based Nu_{hnf} may not be applicable for hybrid nano-oils, which are analyzed in sub-section 4.2 of the chapter. Furthermore, all the developed Nu_{hnf} correlations are nanoparticle-specific, and the use of these needs suitable property correlations. Hence, the developed separation approach helps address this important research gap. As discussed, the effect of the nanoparticle is isolated from the base fluid on Nu_{hnf}. The chapter presents (a) deduction of a generalized Nusselt number correlation for hybrid nanofluids (Nu_{gen}), using the separation approach for water-based and oil-based hybrid nanofluids, and (b) CFD analyses for turbulent heat transfer in a long, straight, circular tube for the assessment of developed Nu_{gen}.

4.1 Hybrid Nanofluids

The thermophysical properties of hybrid nanofluids depend on particle types (metal, oxide, Carbon-Nanotube, and graphene nanoplatelet), particle shape (spherical, cylindrical, and platelet), particle diameter (1-100 nm), particle-particle interaction, particle concentration, and the base fluid. The thermophysical properties of pure fluids are adopted from the Engineering Equation Solver [97]. The experiment-based thermophysical properties of hybrid nanofluids and geometrical properties of nanoparticles are obtained from the various literature [43][55][57][71][72][73][74][97][118][119].

4.1.1 Nusselt Number Correlations for Hybrid Nanofluids: A Comparative Assessment

As discussed, the widely-tested Gnielinski's [63] *Nu* correlation for pure-fluid is valid for $0.5 \leq Pr \leq 2000$ and $3 \times 10^3 < Re < 5 \times 10^5$ (see Table 2.1). This correlation applies to Therminol and vegetable oils. A review of the reported water-based Nu_{hnf} for turbulent flow is provided in the literature survey (see Table 2.2). These correlations are defined as functions of Re_{hnf}, $Pr_{hnf,}$ and φ. The selection of Nu_{hnf} considers chronological development, power-law type expressions, shape, size, and combinations of different nanoparticles, for turbulent flow with $10000 < Re_{hnf} < 30000$, are summarized in Table 2.2. A careful investigation of these correlations reveals that the exponents of Pr_{hnf} are between -0.9 to 1.6, and the exponents of Re_{hnf} are between 0.8 to 1.15. This means that for a given Re_{hnf}, the variation of Nu_{hnf} strongly depends on $Pr_{hnf.}$ Therefore, a preliminary assessment of different Nu_{hnf} is performed for hybrid nanofluids like ND-Ni-water, MWCNT-Fe_3O_4-water, and rGO-Co_3O_4-water (see Figure 4.1). These include different nanoparticle types, shapes, and combinations. The analysis reveals that Nu_{hnf}, as in Suresh et al. [73], Sundar et al. [71][55], Madhesh et al. [74], Yarmand et al. [72], and Minea et al. [57], predict the experiments mostly within ±20%. A wide variation among the correlations, exceeding 40%, is inferred for all the hybrid nanofluids. However, the correlations as in Sundar et al. (2014) [71] and Sundar et al.(2018) [55] show a better predictive capability for Nu_{hnf} with different nanoparticles; however, these correlations are nanofluid-specific and property correlation-dependent. This motivates the development of a separation-based generalized Nu_{hnf} for water, oil, and different nanoparticles. The approach is discussed subsequently.

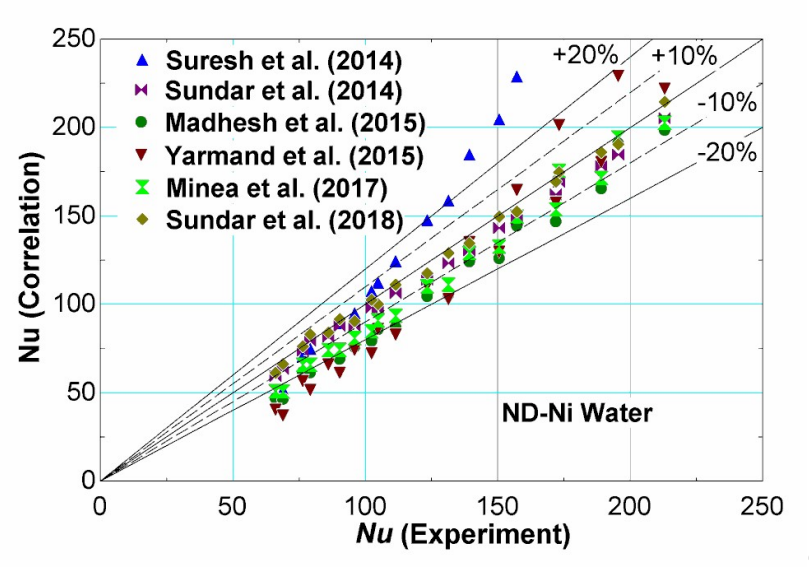
Suresh et al. (2014)
Sundar et al. (2014)
Madhesh et al. (2015)
Yarmand et al. (2015)
Minea et al. (2017)
Sundar et al. (2018)
+20%
+10%
-10%
-20%
ND-Ni Water
Nu (Correlation)
Nu (Experiment)
0
50
100
150
200
250

(a)

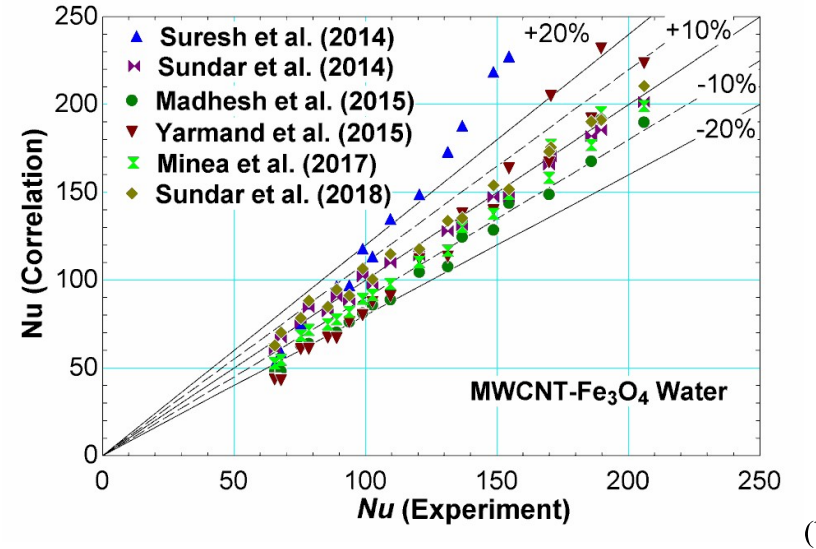
Suresh et al. (2014)
Sundar et al. (2014)
Madhesh et al. (2015)
Yarmand et al. (2015)
Minea et al. (2017)
Sundar et al. (2018)
+20%
+10%
-10%
-20%
MWCNT-Fe3O4 Water
Nu (Correlation)
Nu (Experiment)
0
50
100
150
200
250

(b)

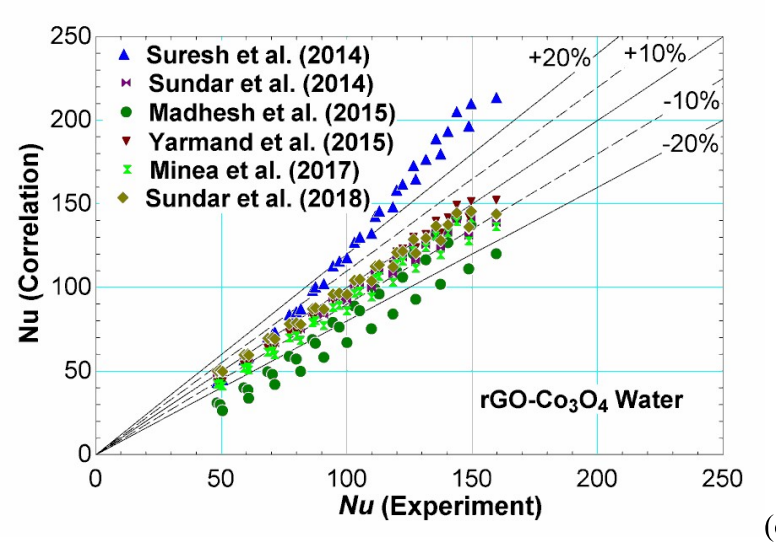

(c)

Figure 4.1 Comparison of water-based Nu_{hnf} for (a) ND-Ni (spherical-spherical) (b) MWCNT-Fe_3O_4 (cylindrical–spherical), (c) rGO-Co_3O_4 (platelet-spherical) nanoparticles for 2300 < Re_{hnf} < 22000, *4*< Pr_{hnf} < 8 and 20 ºC < T < 80 ºC.

4.1.2 Separation Approach: Generalized Nusselt Correlation for Hybrid Nanofluids

As discussed, the separation approach isolates the effect of nanoparticles on Nu_{hnf} from the base fluid. The effect of base fluid (in Nu_{hnf}) is incorporated using a well-known correlation (Nu_{bf}). Therefore, Nu_{hnf} is expressed using equation 4.1, where η represents the correction factor for hybrid nanoparticles.

$$\underbrace{Nu_{hnf}}_{\substack{\text{to be selected for}\\ \text{nanofluids from literature}\\ (\textbf{which correlation}??)}} = \underbrace{\eta}_{\substack{\text{for the separate effect}\\ \text{of nanoparticles}\\ (\textbf{unknown correction factor})}} \underbrace{Nu_{bf}}_{\substack{\text{selected to account}\\ \text{for base−fluid flow}\\ (\text{known},\textbf{Gnielinski})}} \tag{4.1}$$

$$\text{where,} \quad \eta = C_1 \alpha_r^{C_2} \phi^{C_3} n^{C_4}$$

Here, $\alpha_r = \frac{\alpha_p}{\alpha_{bf}}$ is the effective thermal diffusivity ratio, *n* is the shape factor, $\phi$is the volume fraction of nanoparticles. In equation 4.1 Nu_{hnf} is required for calculating η. Based on the comparative assessment, the experiment-based correlation from Sundar et al. (2014) [71] and (2018) [55] is preferred for Nu_{hnf}, which is applicable

for different nanoparticles. The well-known Gnielinski correlation [63] is selected for Nu_{bf}, which is appcicable for 3000 < *Re* < 5 x 10^5 and 0.5 < *Pr* < 2000, and accounts for the turbulent flow of oil inside a long tube. Assuming the known Nu_{hnf} and Nu_{bf} in equation 4.1, the developed regression analysis for estimating coefficients C_1 to C_4 in η, is described in Chapter 3 (see section 3.1.3.3). The final form of separation-based generalized Nusselt number correlation for hybrid nanofluids will be as follows:

$$Nu_{gen} = \underbrace{C_1 \alpha_r^{C_2} \phi^{C_3} n^{C_4}}_{known} \underbrace{Nu_{bf}}_{\text{(known, Gnielinski)}} \tag{4.2}$$

Here, the subscript *gen* is used to distinguish the *separation-based generalized Nusselt number correlation for hybrid nanofluids* from the *experiment-based* Nu_{hnf} from Sundar et al. [71][55]. The need and benefits of the approach will be discussed in section 4.3. The major advantage of Nu_{gen} are (a) only the thermophysical and geometrical properties for nanoparticles and thermophysical properties of pure fluids are required, and (b) the applicability for a wide range of fluids, including oil. To the best of the authors' knowledge, no such generalized correlation is reported in the literature for hybrid nanofluids.

4.2 CFD Analysis: Turbulent Forced Convection

Thermal oils are widely used as HTF in CST systems. Recently, an investigation revealed the potential for using less expensive, widely available vegetable oils as alternative HTF in CST systems discussed in chapter 3. There is a dearth of experimental Nu_{hnf} for hybrid nano-oils, which is necessary for validating Nu_{gen}. Therefore, computational fluid dynamics (CFD) analysis is performed with two different hybrid nano-oils, namely, 0.1% Al_2O_3-TiO_2-Therminol55, and 0.8% SiC-TiO_2-diathermic-oil, and for the different heat fluxes ($q^{"}$) 100 and 300 kW/m^2. The motivation for selecting these hybrid nano-oils is the

available experiment-based thermophysical properties [120][121][122]. The problem, numerical methodology, and validation are described subsequently.

4.2.1 Problem Description

A two-dimensional axis-symmetric computational domain is selected to calculate Nu_{hnf} for hybrid nano-oils (see Figure 4.2). The selection of this problem is motivated by (a) the planned laboratory experiment with oil, having unheated tube length = 1.5 m, heated tube length = 2.0 m, inner tube diameter (D) = 0.0285 m, and tube length (L) to diameter ratio $L/D \cong$ 123, and (b) the available experimental Nusselt number correlation (Nu_x) [123], for unheated tube length = 3.28 m, heated tube length = 6.37m, and inner tube diameter = 0.01016 m. The unheated tube generates the fully-developed inflow condition for the heated tube to attain the thermally fully-developed condition. The heat transfer analysis is performed using ANSYS-FLUENT version 19.2. The numerical modeling framework is described subsequently.

One of the generated structured grids for CFD modeling, including boundaries, is shown in Figure 4.3. The mesh satisfies $y^+ = 1$ for the first point near the wall. This means the viscous boundary layer is well resolved. The generated different meshes, including the grid size and the number of computational elements, are summarized in Table 4.1. The coarse and very fine grids comprise 17500 and 350000 computational elements, respectively.

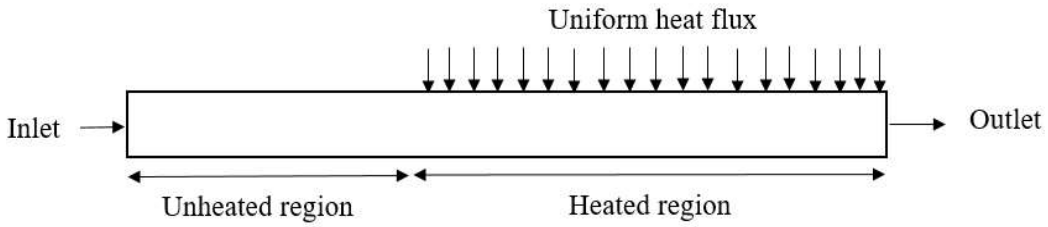

Figure 4.2 A 2D, axisymmetric schematic of the computational domain for CFD analysis.

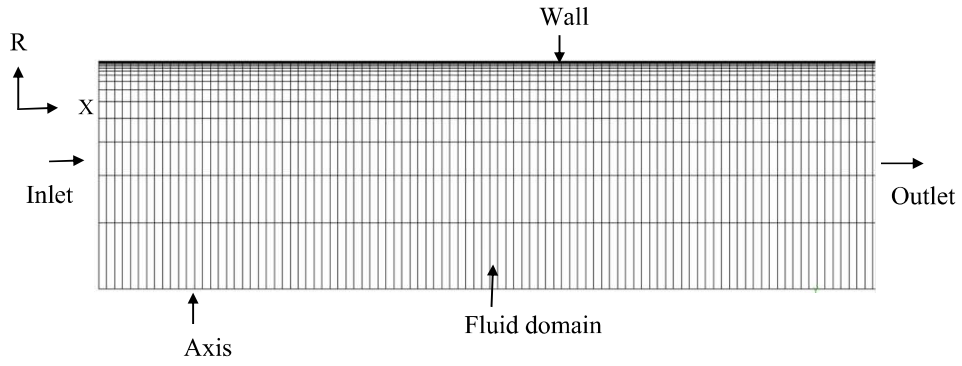

Figure 4.3 An example of the generated structured mesh with $y^+ = 1$ for a well-resolved flow field.

Table 4.1 The generated grids and calculated $\overline{Nu}$ using CFD modeling.

Grid	Grid size (mm)	Generated mesh	Number of elements	Average Nusselt Number ($\overline{Nu}$)
Coarse	2	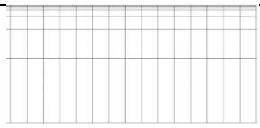	17500	207.67
Medium	1	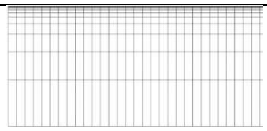	52500	203.74
Fine	0.5	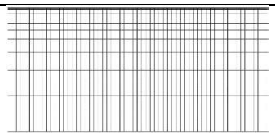	140000	202.39
Very Fine	0.25	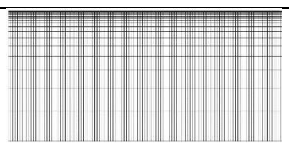	350000	201.84

4.2.2 Mathematical Modeling

Generally, single-phase or multi-phase approaches for modeling the transport phenomena of nanofluids, assuming the homogeneity of dispersed nanoparticles [41]. The base fluid and nanoparticles are assumed to be in thermal equilibrium and flow with the same local velocity for the single-phase model. For the multi-phase approach, base fluid and nanoparticles are treated as separate phases. In this work, the single-phase approach is adopted for the heat transfer analysis, with the turbulent flow of hybrid nano-oil, through a straight, horizontal, long tube. This is described subsequently.

4.2.2.1 Governing Equations and Turbulence Modeling

The single-phase, 2D, axis-symmetric numerical model assumes that (a) the fluid is incompressible and Newtonian for a low volumetric concentration of nanoparticles, (b) the viscous dissipation is negligible, and (c) the pipe is smooth. The following Reynolds-Averaged Navier-Stokes (RANS) equations, including energy, for turbulent fluid flow and heat transfer at the steady state, are reproduced from [124]:

Continuity equation:

$$\nabla \cdot (\rho \overline{U}) = 0 \tag{4.3}$$

Momentum equation:

$$\nabla \cdot (\rho \overline{U}\,\overline{U}) = -\nabla(\bar{P}) + \mu \nabla^2 \overline{U} - \nabla \cdot (\rho \overline{u'u'}) \tag{4.4}$$

Energy equation:

$$\nabla \cdot \left(\rho c_p \overline{U}\,\overline{T}\right) = -\nabla \cdot (k\,\nabla \overline{T} \; - \rho c_p \overline{u'T'}) \tag{4.5}$$

where $\bar{P}$,$\overline{T}$, and $\overline{U}$are the time-averaged pressure, temperature, and velocity, respectively; T' and $u'$are the fluctuations in temperature and velocity, respectively; $\rho c_p \overline{u'T'}$ and $\rho \overline{u'u'}$ are the turbulent heat fluxes and turbulent shear stress, respectively. The turbulent kinetic energy (K) and dissipation rate of turbulent kinetic energy (ε) based turbulence models were selected for comparative assessment, using Al_2O_3-EG/water

mixture (60:40), Al_2O_3-water and TiO_2-water are reported in [125][126][40]. They suggested the use of standard K- ε (SKE) and realizable K- ε (RKE) models. The SKE model is as follows [127][128]:

$$\nabla \cdot(\rho \overline{U} K) = \nabla \cdot \left\{\left(\frac{\mu_t}{\sigma_K}\right) \nabla(K)\right\} + 2\mu_t \mathrm{S}_{ij}.\mathrm{S}_{ij} - \rho\varepsilon \tag{4.6}$$

$$\nabla \cdot(\rho \varepsilon \overline{U}) = \nabla \cdot \left\{\left(\frac{\mu_t}{\sigma_\varepsilon}\right) \nabla(\varepsilon)\right\} + C_{1\varepsilon} \frac{\varepsilon}{k} 2\mu_t \mathrm{S}_{ij}.\mathrm{S}_{ij} - C_{2\varepsilon} \rho \frac{\varepsilon^2}{K} \tag{4.7}$$

$$\mu_t = \rho C_\mu \frac{K^2}{\varepsilon} \tag{4.8}$$

In equations 4.6 – 4.8, $S_{i,j}$ represents the modulus of the mean rate of the strain tensor, σ_K and σ_ε are the turbulent Prandtl number for K, ε, respectively, and μ_t is modeled as in equation 4.8. Suggestions are provided for improvement in the SKE model for different sets of coefficients (see Table 4.2). Here, $C_\mu \approx 0.9,\ 1.44 \leq C_{\varepsilon 1} \leq 1.5, 1.83 \leq C_{\varepsilon 2} \leq 1.92, 1.0 \leq \sigma_K \leq 1.4, 1.3 \leq \sigma_\varepsilon \leq 1.4$. These are identified with SKE-AB, SKE-LB, SKE-LS, and SKE-AKN. It is evident from Table 4.2 that the model coefficients for SKE-LB are well in the considered range for simulations. Thus, separate simulations using SKE-LB are not performed.

The Realizable K-ε model (RKE)includes the following equations [128]:

$$\nabla \cdot(\rho \overline{U} K) = \nabla \cdot \left\{\left(\mu + \frac{\mu_t}{\sigma_K}\right) \nabla(K)\right\} + G_\kappa - \rho\varepsilon \tag{4.9}$$

$$\nabla \cdot(\rho \varepsilon \overline{U}) = \nabla \cdot \left\{\left(\mu + \frac{\mu_t}{\sigma_\varepsilon}\right) \nabla(\varepsilon)\right\} + \rho C_1 \mathrm{S}_\varepsilon - \rho C_2 \frac{\varepsilon^2}{\mathrm{K} + \sqrt{\nu\varepsilon}} \tag{4.10}$$

$$C_1 = max\left[0.43, \frac{\eta}{\eta + 5}\right], \eta = S\frac{\mathrm{K}}{\varepsilon}\ and\ S = \sqrt{2S_{ij}S_{ij}} \tag{4.11}$$

$$\text{where}, \mu_t = \frac{\rho \mathrm{K}^2}{\varepsilon}\left(A_0 + A_s \frac{\mathrm{K}U^*}{\varepsilon}\right)^{-1} \tag{4.12}$$

In equations 4.9 - 4.12,G_κ is the production term for K, $\sigma_K = 1.0$ and $\sigma_\varepsilon = 1.2$, μ_t is the modeled eddy viscosity using A_0= 4.04, and A_s=$\sqrt{6}\cos\theta$ for$\theta = \frac{1}{3}\cos^{-1}(\sqrt{6}\ W)$and C_2=1.9. The approximations for μ_t are different in SKE and RKE.

Table 4.2 The adopted coefficients for CFD simulation with the SKE model [125].

Model and coefficients [125]	C_μ	$C_{\varepsilon 1}$	$C_{\varepsilon 2}$	σ_k	σ_ε
Abid (SKE-AB)	0.09	1.45	1.83	1.0	1.4
SKE-LB	0.09	1.44	1.92	1.0	1.3
Launder and Sharma (SKE-LS)	0.09	1.44	1.92	1.0	1.3
Abe et al. (SKE-AKN)	0.09	1.50	1.90	1.4	1.4

4.2.3 Boundary Conditions and Numerical Scheme

For solving the coupled, nonlinear partial differential equations, the applied boundary conditions are (a) inlet: spatially uniform velocity U_{in} and temperature T_{in}, (b) outlet: zero velocity gradient, zero temperature gradient, P_{guage}=0, and the turbulence intensity at the inlet and outlet are as follows:

$$I = 0.16\, Re^{(-\frac{1}{8})} \tag{4.13}$$

where Re is calculated using U_{in} and the hydraulic diameter, D_h= 0.0285 m, (c) wall: adiabatic boundary condition on the unheated section and uniform heat flux on the heated section. The Reynolds-averaged equations for continuity, momentum, energy, K, and ε are discretized using the second-order upwind scheme. The semi-implicit pressure-linked equations (SIMPLE) method is solved for pressure-velocity coupling. The measured, temperature-dependent, thermophysical properties for 0.1% Al_2O_3-TiO_2-Therminol55 and 0.8 % SiC-TiO_2-Diathermic-oil are taken from [120][121][122]. The convergence criteria for the scaled residuals of time-averaged- velocity, temperature, K, and ε are set to be 10^{-6}.

4.2.4 Grid Independence Test and Validation

4.2.4.1 Grid Independence Test

The 2D experimental geometry with L/D≅ 123 is selected for the grid independence analysis, and the grid size is varied from 2 mm to 0.25 mm (Table 4.1). The numerical simulations are performed with Therminol55 oil for Re = 10000 and $q^{"} = 300$ kW/m^2. The calculated $\overline{Nu}$ in the thermally fully developed region, for $2.0 \leq x \leq 3.5$, are summarized in Table 4.1. A detailed discussion is provided in section 4.3.1. The relative deviation between the medium grid (1 mm size) and the very fine grid (0.25 mm size) is less than 1 %, which is acceptable for the current purpose. Therefore, the fine grid (0.5 mm size) is selected for further analysis.

4.2.4.2 Validation

This sub-section deals with the validation of the CFD approach for water and oil, with experiments and Nusselt number correlations. These are presented subsequently.

4.2.4.2.1 Assessment using Nu_x for Water

Choi et al. [123] experiment with water as HTF is selected for validation exercise with T_{in} = 293.15 K, U_{in} = 1.9 – 2.0 m/s, $q^{"} = 45.2$ kW/m^2 for an input power of 9.19 kW and $q^{"}$ = 61.8 kW/m^2 for an input power of 12.56 kW. The reported Nu_x in equation 4.19 depends on local Reynolds number (Re_x) and Prandtl number (Pr_x). The variation in Nu_x is attributed to the local thermophysical properties of the fluid. These are depicted in Figure 4.4.

$$Nu_x = 0.00425\, Re_x^{0.979} Pr_x^{0.4} \left(\frac{\mu_w}{\mu_b}\right)^{-0.11} \tag{4.14}$$

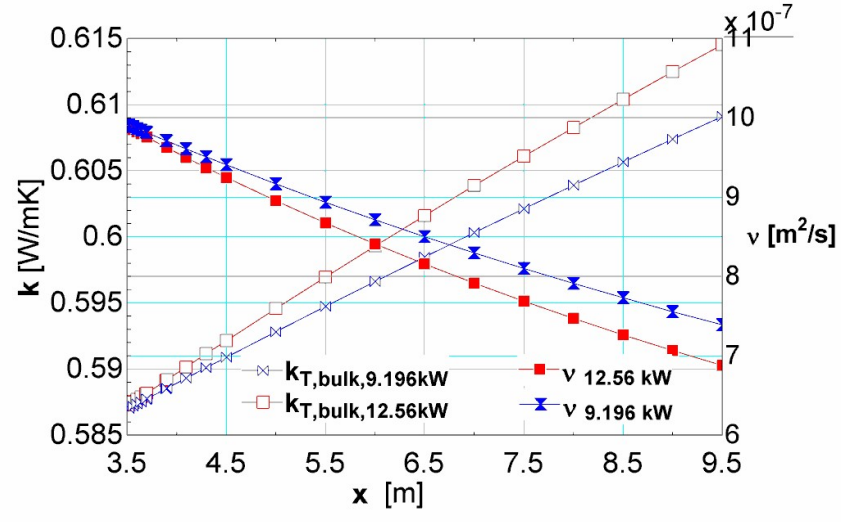

Figure 4.4 Variation of thermal conductivity and kinematic viscosity with local bulk mean temperature and input power along the axial direction.

In the redeveloping region, fluid viscosity decreases with increasing temperature and q'' along the axial flow direction (see Figure 4.4). The fluid thermal conductivity increases with temperature and q'' along the flow direction. Therefore, Re_x and Pr_x will depend on the applied heat flux for a given inflow condition. Consequently, the range of Nu_x will be different for different heat fluxes. These will be investigated subsequently.

A comparison between the computed values for Nu_x using RKE, SKE-AB, SKE-LS, and SKE-AKN models, and the Choi et al. [123] correlation is shown in Figure 4.5. The analyses reveal the following:

(a) The computed values for Nu_x, using the different turbulence models, are comparable in the thermally fully developed region (Figure 4.5a). Therefore, any of these models can be employed for numerical simulation.

(b) The calculated maximum, relative differences between computed and correlation for Nu_x are between 3.5 – 4.2% (Figure 4.5b), which is suitable for practical purposes. Thus, for the subsequent analysis, the RKE model is selected.

(c) For an input power of 9.19 kW, the obtained maximum Re_x= 26000, and for an input power of 12.56 kW, the obtained maximum Re_x= 30500 (Figure 4.5c). Therefore, it is inferred that the values for Re_x increases with q'', which is attributed to the local thermophysical fluid properties of water (Figure 4.4).

(d) The values for Nu_x, at a given Re_x, increases with input power or q''. This is depicted by the vertical dotted line in Figure 4.5c. This is attributed to the varying Pr_x for water flow along the direction.

The validation exercise concludes that (a) the numerical framework is acceptable for further investigation, (b) the selection of the Choi et al. [123] correlation is appropriate for Nu_{bf} in equation 4.2. Therefore, the applicability of Choi et al. [123] correlation for oil is tested subsequently.

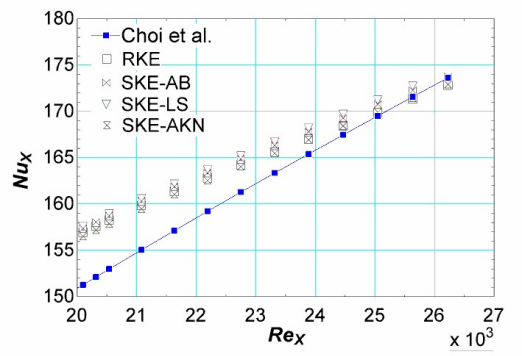

(a)

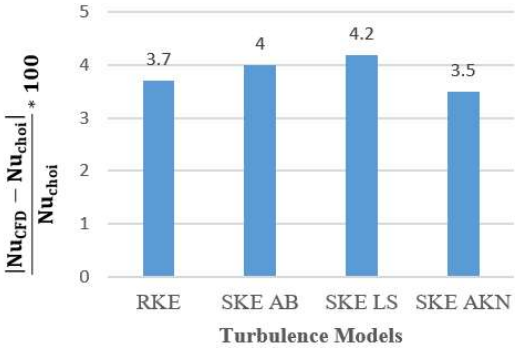

(b)

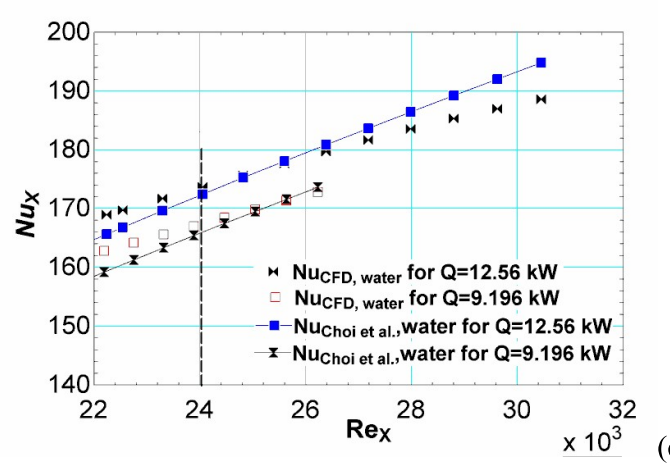

(c)

Figure 4.5(a) A comparison between CFD and Choi et al. [123] Nu_x for 20000 < Re_x < 31000 and 3 < Pr < 7, using different turbulence models, at an input power of 9.19 kW, (b) the maximum, relative, percentage deviation between the computed and correlation-based values for Nu_x, using the different turbulence models, and (c) the computed and correlation-based values for Nu_x, using the RKE turbulence model and different input powers.

4.2.4.2.2 Assessment using $\overline{Nu}$ for Oil

The CFD-based $\overline{Nu}$ is compared for Gnielinski and Choi correlation for Therminol55 oil (see Figure 4.6). The maximum relative deviation between Gnielinski and computed $\overline{Nu}$ is about ±8%, for $q^{"}$ = 100 kW/m^2 and 300 kW/m^2, 100 ºC < T < 143 ºC, 11000 < Re_{bf} < 34000 and 38 < Pr < 44. The differences using the Choi correlation exceed 40%. Therefore, the Gnielinski correlation for Nu_{bf} is selected in equation 4.2 to estimate Nu_{gen}.The need and benefits of the separation approach are discussed subsequently.

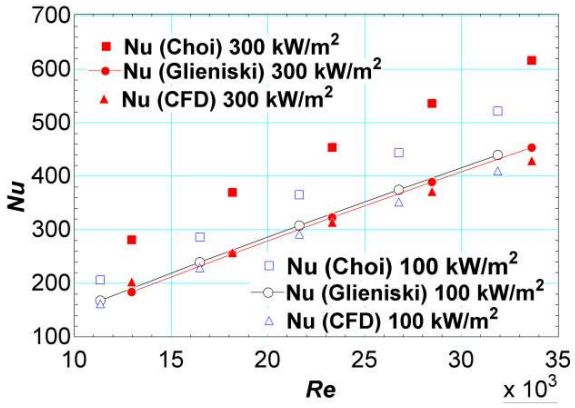

Figure 4.6 A comparison between the computed and correlation-based (Choi and Gnielinski) $\overline{Nu}$, for Therminol55 oil with q''= 100 kW/m^2 and 300 kW/m^2, 100 ºC < T < 143 ºC, 11000 < Re_{bf} < 34000 and 38 < Pr < 44.

4.3 Results and Discussion

This section describes (a) the computed hydro-thermal development of turbulent oil flow, (b) the need for separation-based Nu_{gen} for hybrid nano-oils, and (c) the assessment of Nu_{gen} for water and oil.

4.3.1 Hydro-Thermal Development of Turbulent Oil Flow

The CFD analyzed non-dimensional axial velocity ($u^* = u/u_{max}$) for Therminol55 oil, at several axial positions, are plotted to depict the flow development (see Figures 4.7a and 4.7b). Here, the planned laboratory experiment with $L/D \cong 123$ and q''= 300 kW/m^2 is selected with 100 ºC < T < 143 ºC, 11000 < Re_{bf} < 34000 and 38 < Pr < 44. The computed values for u^* at x = 1.2 m and 1.5 m are practically the same. Therefore, the fully-developed inflow condition to heated length is attained. A noticeable change in $u^*|_{x>1.5\ m}$ reveals the redeveloping flow field, consistent with Choi et al. [123]. This is attributed to the continuous change in thermophysical fluid properties due to heating along the flow

direction (analogous to Figure 4.4). The non-dimensional fluid temperature in Figures 4.7c and 4.7d is given by $T^* = \frac{T_s(x)-T(r,x)}{T_s(x)-T_m(x)}$, where $T_s(x)$ is the wall temperature and $T_m(x)$ is the bulk mean fluid temperature at x,$T(r,x)$is the fluid temperature at(r,x). The practically same T^* for $2.0 \leq x \leq 3.5$ reveals that thermal development is attained. Therefore, the heated region, $2.0 \leq x \leq 3.5$, is selected for computing $\overline{Nu}$. This is required for comparative assessment of Gnielinski and Choi correlations to select Nu_{bf} for thermal oil.

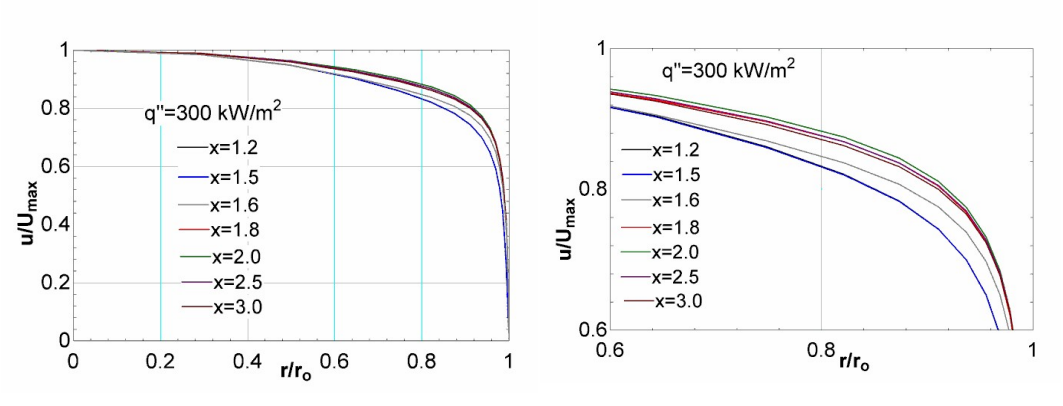

(a) (b)

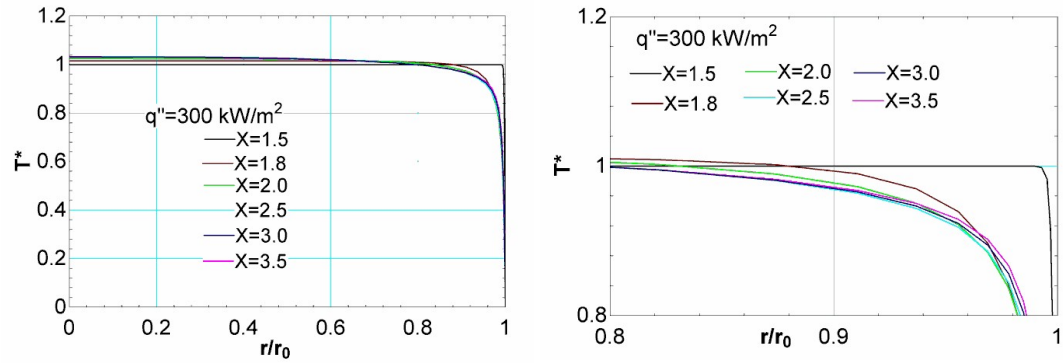

(c) (d)

Figure 4.7 Non-dimensional (a) velocity profiles, (b) zoom-in view of velocity profiles, (c) temperature profiles, and (d) zoom-in view of temperature profiles, for Therminol55 oil with 100 ºC < T < 143 ºC, 11000 < Re_{bf} < 34000 and 38 < Pr < 44.

4.3.2 Separation-based Nu_{gen}: Need and Assessment

A comparison between the computed Nu_{hnf} and experimental Nu_{hnf} from Sundar et al. [71][55] for 0.8% SiC-TiO_2-diathermic-oil is provided in Figure 4.8 with 100 ºC < T < 113 ºC, 10000 < Re_{hnf} < 31000 and 69 < Pr < 76. The assessment reveals that the water-based Nu_{hnf} substantially over-predicts the CFD-based values for hybrid nano-oils by about 60-100% as explained in the introduction. This is attributed to the very different Pr ~ 5-6 for water and Pr ~ 45-55 for pure oils. This means, separating the effect of nanoparticles and base fluid on Nu_{hnf} is a probable solution.

Considering the discussion in sub-sections 4.1.1 and 4.1.2, the experimental Nu_{hnf} from Sundar et al. [55] for case 1 and Sundar et al. [71] for case 2 are selected as LHS in equation 4.1 to obtain the correction factor η, for different nanoparticles. The computed values C_1, C_2, C_3, and C_4 equation 3.4 is obtained and summarized in Table 4.3, including the corresponding R^2 values.

Finally, the generalized Nusselt number correlation for hybrid nanofluids (Nu_{gen}) is expressed as follows:

$$Nu_{gen} = \underbrace{c_1 \alpha_r^{C_2} \phi^{C_3} n^{C_4}}_{\eta} \underbrace{\left\{ \frac{\frac{f}{8}(Re - 1000)Pr}{1 + 12.7\sqrt{\frac{f}{8}}\left(Pr^{\frac{2}{3}} - 1\right)} \right\}}_{\textbf{Gnielinski correlation, } Nu_{bf}} \text{ for } 0.5 \leq Pr \leq 2000 \tag{4.15}$$

The major advantages associated with Nu_{gen} are (a) Gnielinski correlation for Nu_{bf} valid for $0.5 \leq Pr \leq 2000$, and (b) only the thermophysical and geometrical properties of nanoparticles are needed. *Thus, it may be concluded that Nu_{gen} will be applicable for water and oil-based hybrid nanofluids with different combinations of nanoparticles.* This is presented subsequently.

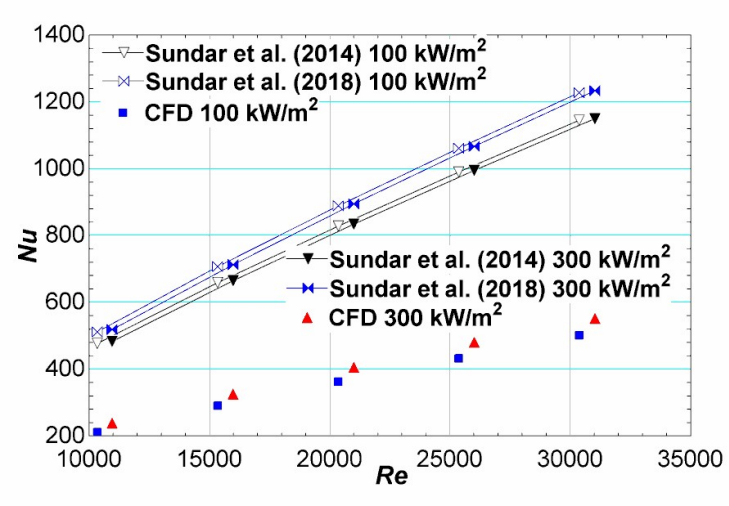

Figure 4.8 A comparison between CFD and Sundar et al. (2014, 2018) [71][55] for Nu_{hnf} using SiC-TiO_2-diathermic oil and different heat fluxes 100 and 300 kW/m^2 with 100 ºC < T < 113 ºC, 10000 < Re_{hnf} < 31000 and 69 < Pr < 76.

Table 4.3 The computed coefficients for η using the experimental Nu_{hnf} and R^2 value.

Nu_{gen}	C_1	C_2	C_3	C_4	R^2
case 1	1.01	0.07612	0.04403	-0.1457	0.885
case 2	1.01	0.08879	0.0542	-0.1482	0.919

4.3.2.1 Assessment with Water-Based Hybrid Nanofluids

The deduced Nu_{gen} for hybrid nanofluids, case 1 and case 2, are compared using the experimental data for rGO-Co_3O_4-water. Figure 4.9a shows that the calculated Nu_{gen} reproduces the experiments, and the computed values are comparable. However, because of a marginally better value of R^2, Nu_{gen} for case 2 is selected for further assessment with water-based hybrid nanofluids. Figure 4.9b reveals that Nu_{gen} predicts the experimental values, for Al_2O_3-Cu-water, GNP-Ag-water, Graphite-SiO_2-water, MWCNT-Fe_3O_4-water, ND-Ni-water, and rGO-Co_3O_4-water, mostly within ±10-20%.The assessment of $Nu_{gen}$for hybrid nano-oils is performed subsequently.

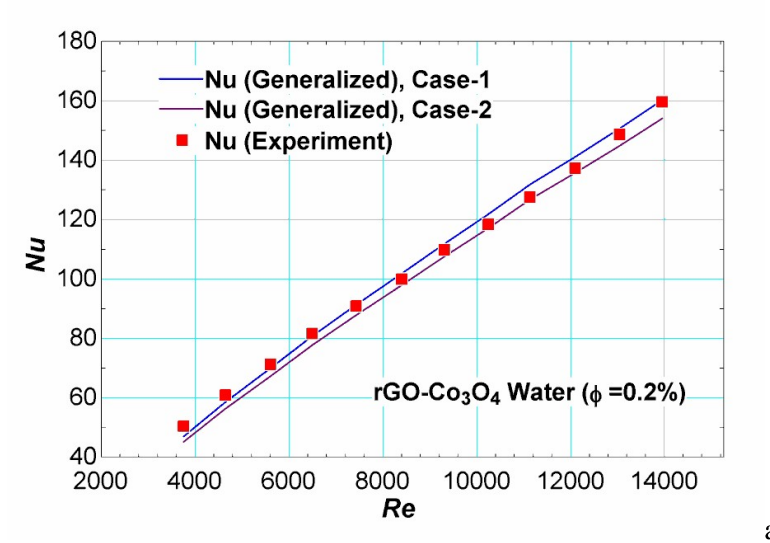

a)

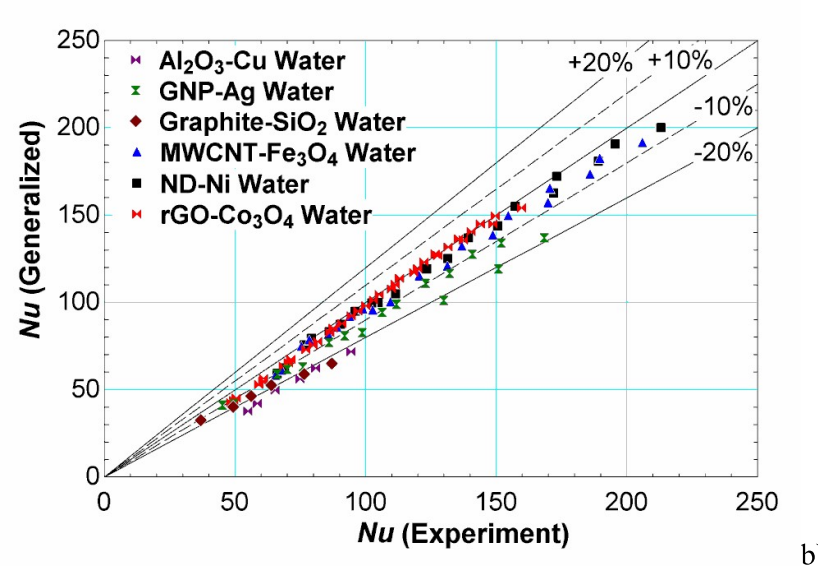

b)

Figure 4.9 Comparison between the experimental and Nu_{gen} in equation 4.15 for (a) rGO-Co_3O_4-water, and (b) Al_2O_3-Cu-water, GNP-Ag-water, Graphite-SiO_2-water, MWCNT-Fe_3O_4-water, ND-Ni-water, and rGO-Co_3O_4-water for 2300 < Re_{hnf} < 22000, 20 ºC < T < 80 ºC and 4 < Pr_{hnf} < 8.

4.3.2.2 Assessment with Hybrid Nano-Oils

Two different hybrid nano-oils, Al_2O_3-TiO_2-Therminol55and SiC-TiO_2-Diathermic-oil, are selected for the final assessment of Nu_{gen}. Therminol/diathermic oils are widely utilized

for heat transfer in PTC absorbers, and the *Pr* for these oils is much higher than water. CFD simulations are performed with these hybrid nano-oils for $100\ ^{o}\text{C} < T < 130\ ^{o}\text{C}, 10000 < Re_{hnf} < 31000$ and $48 < Pr < 76$. The estimated Nu_{gen} equation 4.15 is compared with the corresponding CFD values (see Figure 4.10). The deduced Nu_{gen} predicts the computed values for hybrid nano-oils mostly within $\pm$10-20%. Further analyses reveal Nusselt number enhancement by about 20-25% for hybrid nano-oils compared to pure oils. These findings allow concluding a) the Nu_{gen} will be helpful in heat transfer analysis with hybrid nano-oils, and b) the hybrid nano-oils will be beneficial for CST systems.

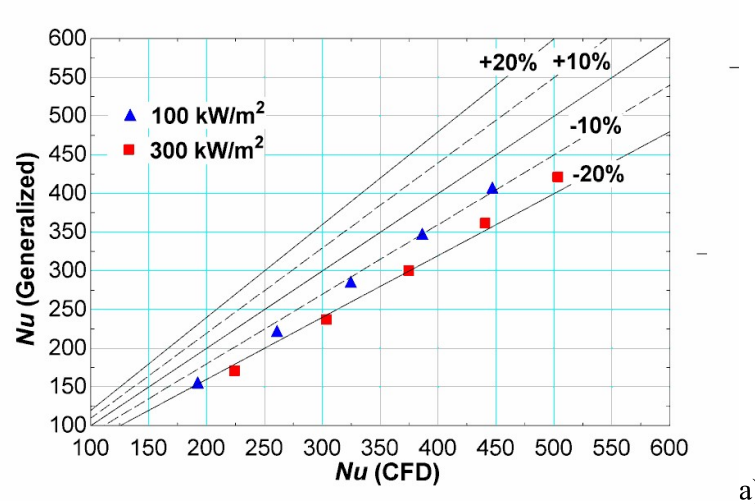

a)

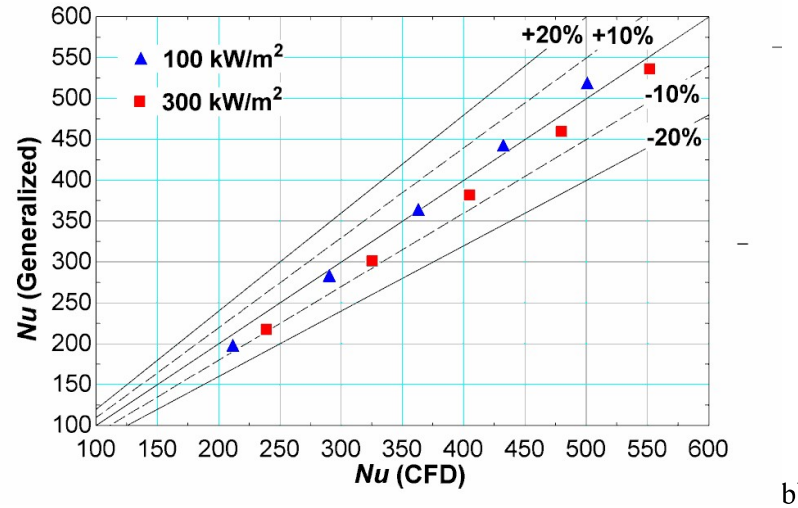

b)

Figure 4.10 A comparison of the estimated Nu_{gen}, using case 2 in equation 4.15 with CFD analysed values, for (a) Al_2O_3-TiO_2-Therminol 55 with 100 ºC < T < 130 ºC, 10000 < Re_{hnf} < 31000 and 46 < Pr_{hnf} < 54 and (b) SiC- TiO_2-Diathermic-oil with 100 ºC < T < 113 ºC, 10000 < Re_{hnf} < 31000 and 69 < Pr_{hnf} < 76.

4.4 Summary

Hybrid nano-oils are being investigated as HTF for concentrated solar thermal systems, for example, in PTC absorbers, to enhance thermal efficiency. Water-based Nusselt number correlations for hybrid nanofluids substantially over-predict the values for hybrid nano-oils by about 60-100%. Therefore, the development of separation-approach-based generalized Nusselt number correlation for hybrid nanofluids is undertaken. In this approach, the effect of base fluid and nanoparticles are separated. The effect of base fluid is incorporated using the Gnielinski correlation for the Nusselt number (Nu_{bf}), and the effect of nanoparticles is incorporated as a correction factor η. The proposed generalized correlation for the thermally fully developed flow condition of hybrid nanofluids is as follows:

$$Nu_{gen} = \underbrace{c_1 \alpha_r^{C_2} \phi^{C_3} n^{C_4}}_{\eta} \quad \underbrace{\left\{ \frac{\frac{f}{8}(Re-1000)Pr}{1+12.7\sqrt{\frac{f}{8}}\left(Pr^{\frac{2}{3}}-1\right)} \right\}}_{\textbf{Gnielinski correlation, } Nu_{bf}} \qquad \begin{matrix} \text{for } 0.5 \leq Pr \leq 2000 \\ 10000 < Re < 30000 \end{matrix}$$

where the coefficients C_1, C_2, C_3, and C_4, are obtained using the Nusselt number correlation from Sundar et al. [55][71]. The assessment of Nu_{gen} using water and oil-based hybrid nanofluids reveals the following:

a) Nu_{gen} predicts the experimental values, for Al_2O_3-Cu-water, GNP-Ag-water, Graphite-SiO_2-water, MWCNT-Fe_3O_4-water, ND-Ni-water, and rGO-Co_3O_4-water, mostly within ±10-20%.

b) Nu_{gen} predicts the computed values, for Al_2O_3-TiO_2-Therminol55 and SiC-TiO_2-Diathermic-oil, mostly within ±10-20% for different heat fluxes.It is worth noting that the Prandtl number for water and oils differs substantially.

c) Nu_{gen} provides 20-25 % enhancement in comparison to pure oils. This means the use of hybrid nano-oils will be beneficial for concentrated solar thermal systems.